Distributed optical fibre dynamic magnetic field sensor based on magnetostriction

Ali Masoudi[1, *] and   Trevor P. Newson[1]

[1]*Optoelectronic Research Centre (ORC), University of Southampton, Southampton, SO17 1BJ.*

compiled: March 20, 2014

A distributed optical fibre sensor is introduced which is capable of quantifying multiple magnetic fields along a $1km$ sensing fibre with a spatial resolution of $1m$. The operation of the proposed sensor is based on measuring the magnetorestrictive induced strain of a Nickel wire attached to an optical fibre. The strain coupled to the optical fibre was detected by measuring the strain-induced phase variation between the backscattered Rayleigh light from two segments of the sensing fibre. A magnetic field intensity resolution of $0.3G$ over a bandwidth of of $50Hz$ to $5000Hz$ was demonstrated.

1. Introduction

Magnetic field sensors play an important role in modern society. Their applications vary from monitoring brain activity to measuring the current in high-power transmission lines. Among the various types of magnetic sensors, optical fibre based sensors have attracted a considerable interest due to a number of advantages regarding their sensing range, sensing resolution, and their flexibility. However, the capability of spatially resolving the magnetic field along the entire sensing fibre is what distinguishes distributed optical fibre magnetometer from other techniques.

Distributed optical fibre magnetic-field sensors (DOFMS) are based on monitoring the variation in either the polarization or the phase of the backscattered light from the sensing fibre. DOFMS which are based on the polarization variation exploit the Faraday effect phenomenon which involves the rotation of the plane of polarization of the light propagating inside the fibre. The theoretical principles of this sensor were first elucidated back in 1981 by Rogers [1] and referred to as polarization optical time domain reflectometry (POTDR) and has attracted considerable interest over the years. Recently, experimental results of a state of the art DOFMS were published by Palmieri *el at.* [2] which uses polarization optical frequency domain reflectometry (POFDR) for magnetic field detection. Despite its wide sensing range ($1.5T$), the proposed sensor has a number of limitations including the sensitivity of $100mT$ (which is due to the weak nature of the Faraday effect), the spatial range of $15m$, and repetition rate of $10s$ which makes it suitable only for DC and quasi-DC magnetic field sensing.

Previously reported magnetostrictive-based optical fibre magnetic field sensors are based on coupling an optical fibre to a magnetostrictive material and measuring the magnetic field by monitoring the strain induced on the fibre. Although this technique has been successfully used to develop point sensors using a Mach-Zehnder interferometer (MZI) [3, 4] as well as quasi-distributed sensor using fibre Bragg gratings (FBG) [5, 6], to the best of our knowledge, it has never been employed to develop a DOFMS. In this letter, a distributed magnetic field sensor is demonstrated which is capable of quantifying magnetic fields along a $1km$ of sensing fibre with an spatial resolution of $1m$. The sensing mechanism of the proposed sensor is based on using the distributed dynamic strain measurement technique previously described by Masoudi *et al.* [7] and applying it to an optical fibre which is mechanically coupled to the magnetostrictive material, a Nickel wire.

2. Principles

The principle of operation of the sensor is based on measuring the strain-induced phase variation between the backscattered Rayleigh light from two segments of the sensing fibre. Since the optical fibre is coupled with a magnetostrictive material, the length of it changes in the presence of magnetic field. The relative phase difference between the backscattered lights from the two segments of the fibre, $\Delta\phi$, is a function of the distance between the two segments, L (figure 1). In the absence of a magnetic field, the value of L varies at very low frequency due to ambient temperature variation. In the presence of a magnetic field, however, the value of L changes as a function of the component of the magnetic field parallel to the Nickel wire. Therefore, the measured phase difference between the backscattered light from the two segments within the fibre is a function of the magnetic field.
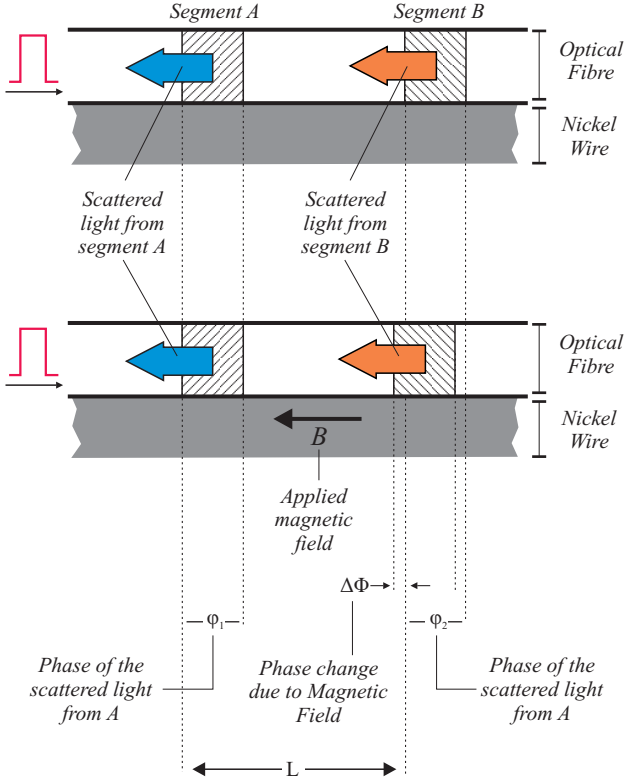
Fig. 1. The effect of magnetic field on the phase of the backscattered light from two separate segments of an optical fibre which is attached to the Nickel wire showing the phase of the backscattered light in the presence and absence of magnetic field.

This phase variation is measured by analyzing the output of an unbalanced MZI using differentiate and cross-multiplying demodulation technique [7]. The length of the MZI path-imbalance, $\triangle\ell$, determines the spatial resolution of the sensor. For a spatial resolution of L meters (i.e. the distance between two segments), the path-imbalance $\Delta\ell = 2L$. A 3×3 coupler is used at the output end of the MZI to eliminate the signal fading problem of a conventional MZI [8]. The intensity of the light at the three output arms of the MZI is given by [7]

$$
\begin{aligned}
I_1 &= I_0[M + N\cos(\Delta\phi)]\\
I_2 &= I_0[M + N\cos(\Delta\phi + \tfrac{2\pi}{3})]\\
I_3 &= I_0[M + N\cos(\Delta\phi - \tfrac{2\pi}{3})]
\end{aligned}
\qquad (1)
$$

where I_0 is the intensity of the input signal and M and N are constant. The output intensities of equation (1) are combined using differentiate and cross-multiplying demodulation to provide an output proportional to $\Delta\phi$ [9]. With an assumption that the Nickel wire is pre-magnetized at the linear region of the magnetostriction curve, the output of the differentiate and cross-multiplying demodulator is

$$
\Phi = \sqrt{3}\Delta\phi = \sqrt{3}\,(\frac{2\pi}{\lambda}\Delta\ell) = 2\sqrt{3}\pi\,\frac{\epsilon_M}{\lambda}\,B \qquad (2)
$$

where λ is the wavelength of the backscattered light, ϵ_M is the magnetostriction constant, and B si the applied magnetic field.

3. Experimental Arrangement
3.A. Experimental Setup
Figure 2 shows a schematic diagram of the experimental setup. A 1550nm distributed feedback (DFB) laser diode was amplitude-modulated to generate $10ns$ pulse at a repetition rate of $10\mu s$. The pulse was then amplified by an Erbium-doped fibre amplifier (EDFA1) to raise the peak power to $4W$. A fibre Bragg grating (FBG1) (Reflectivity 99%; $\Delta\lambda = 3nm$; $\lambda_B = 1550.7nm$) was used to filter the EDFA1 amplified spontaneous emission (ASE) before the amplified pulse was launched into the sensing fibre via circulator C2.

The sensing fibre was formed by adhering $8m$ of single mode optical fibre to $8m$ of Nickel wire ($1mm$ diameter) using epoxy glue. The optical fibre was wrapped around the Nickel wire to prevent the fibre from slipping. The middle $2m$ of the sensing fibre was placed inside two separate 55mm-long solenoid coils (27 turn/mm) as shown in figure 3. The coils were used to generate an AC magnetic field parallel to the direction of the Nickel wire. The rest of the sensing fibre (i.e. $3m$ on either side of the $2m$) was left outside the solenoid coils in order to demonstrate the distributed nature of the sensor. $780m$ and $200m$ of thermally isolated fibres were added before and after the sensing element respectively to form a $1km$ long distributed sensor.

The Rayleigh backscattered light was collected by circulator C2 and amplified by a $25dB$ gain EDFA2. The ASE from this amplifier was filter by FBG2 (Reflectivity 90%; $\Delta\lambda = 1.4nm$; $\lambda_B = 1550.7nm$) before it was fed into a thermally isolated MZI via a 50/50 coupler. The path-imbalance of the MZI was set to $2m$ which corresponds to $1m$ spatial resolution. The light from the three output arms of the MZI were detected using three photoreceivers ($40V/mA$ transimpedance, $125MHz$ bandwidth, $22.5pW/\sqrt{Hz}$ NEP). The output of the photoreceivers were collected by a $250MHz$ oscilloscope at a sampling rate of $625MSa/s$. The phase of the backscattered light was extracted from the collected data using a digitally implemented phase-detector. The signal processing procedure is explained in more details in [7].

3.B. Experimental procedure
A MZI arrangement was initially used to characterize the response of the sensing fibre to the magnetic field for a range of frequencies and intensities. In order to generate the desired magnetic field, two identical driver circuits were used to drive the two solenoids of the experimental setup. The schematic of the driver circuit is shown in figure 4. The circuit was comprised of a signal generator, an emitter-follower amplifier, and an RLC resonant

Fig. 2. Experimental setup. EDFA: erbium-doped fibre amplifier, PD: photodetector, FBG: fibre Bragg grating, DFB: distributed feedback, IS: isolator; V_1 and V_2 ; Outputs of test coils.

Fig. 3. Magnetic field source element used in the experimental setup to generate AC magnetic field.

Fig. 4. Schematic of the circuit used to drive the magnetic coils.

circuit. The inductor L shown in the schematic of figure 4 represents the solenoid inside the experimental setup. The impedance of the serial RLC circuit is minimum at its resonant frequency which is given by $\omega_0 = (LC)^{-1}$. Therefore, to generate a magnetic field at the desired frequencies, different capacitors were used. Test coils were placed inside each solenoid to both monitor and measure the average magnetic field along the axis of the solenoids.

After characterization, the sensing fibre was spliced to the DOFMS setup as shown in figure 2. Although the magnetostriction curve of Nickel wire is an even function

around DC magnetization, the pre-magnetized Nickel wire used in this experiment ensures that the sensing fibre is operating in the linear region of the magnetostriction curve. The driver circuits were initially adjusted to generate $1200Hz$ magnetic field and data was collected for magnetic fields ranging from $1G$ to $8G$ at a repetition rate of $10\mu s$. 20,000 traces were captured during each experimental run which is equivalent to a data acquisition period of $200ms$. To determine the frequency response of the sensor, the driver circuits were modified to generate magnetic fields with a fixed magnitude over a range of frequencies spanning from $50Hz$ to $5000Hz$.
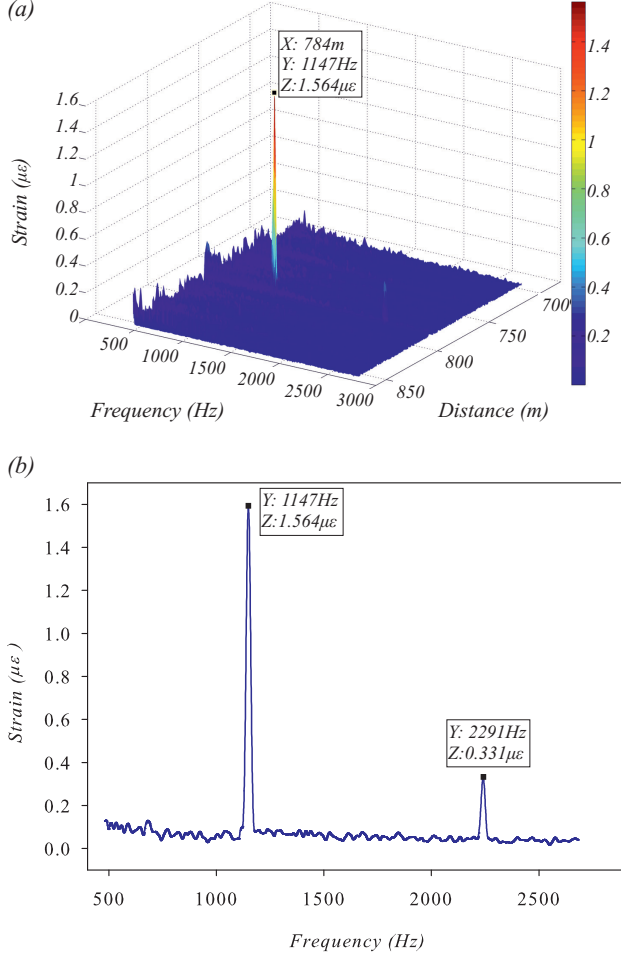
(a)

(b)

Fig. 5. (a) 3D plot of FFT of the phase-detector output for the data points between 700m and 850m. (b) A 2D view of the 3D plot at the location of the peak.

4. Experimental Results

The 3D diagram of figure 5 (a) shows the FFT of the phase detector output for a $1150Hz$ ac magnetic field with a magnitude of $7G$. The two horizontal axes at the bottom of the diagram represent the distance along the sensing fibre and the frequency components of perturbation. The vertical axis of the diagram represents the magnitude of the strain. The peak in this figure indicates a $1147Hz$ sinusoidal perturbation at a distance of $753m$ from the front-end of the sensing fibre. In addition, the amplitude of the peak indicates a strain of $1.56\mu\varepsilon$ in that section of the sensing fibre. For clarity, a 2D view of this 3D plot at the location of the peak is shown in figure 5 (b). A second peak is observed at $2291Hz$, i.e. at the second harmonic of the magnetic field frequency.

Figure 6 shows the response of the sensing fibre to $1200Hz$ magnetic fields at different intensities. The solid line represents the DOFMS output while the dashed line
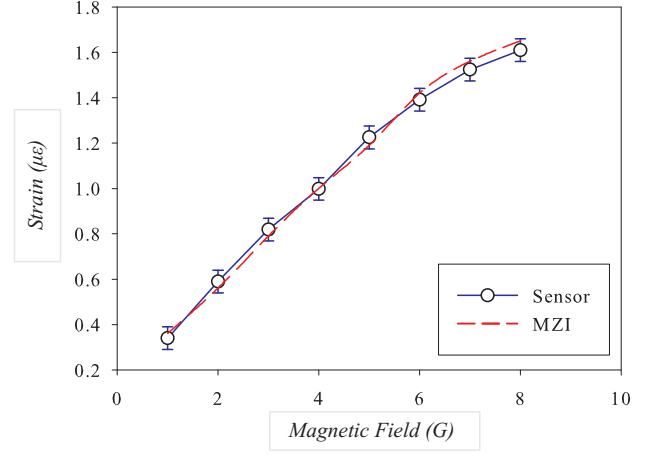

Fig. 6. The response of the sensing fibre to $1200Hz$ sinusoidal magnetic field for a range of different intensities. The solid line shows the DOFMS output while the dashed line represents the the results obtained using MZI.

shows the results obtained using the MZI.

Figure 7 shows the frequency response of the sensing fibre to sinusoidal magnetic fields with a fixed magnitude and a range of frequencies spanning from $50Hz$ to $5000Hz$. The solid line shows the magnetic field-induced strain measured using MZI while the circles are showing the DOFMS output.

5. Discussion

The larger peak in figure 5, accurately indicates the location and the frequency of the applied magnetic field within the resolution of the sensor. In addition, the induced strain of $1.56\mu\varepsilon$ closely matches the results ob-
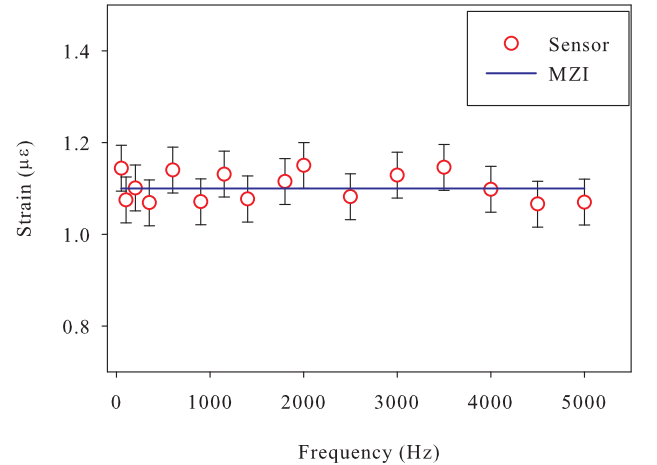

Fig. 7. The response of the sensing fibre to sinusoidal magnetic fields with a fixed magnitude and a range of frequencies spanning from $50Hz$ to $5000Hz$. The solid line shows the magnetic field-induced strain measured using MZI while the circles are showing the DOFMS output.

tained from MZI experiment i.e. a phase-shift of 4π radians for $2m$ of sensing fibre. The smaller peak in figure 5 is the second harmonic of the applied magnetic field. When the magnetic field was switched off, both peaks vanished indicating that the second peak is due to the the presence of the first harmonic in the magnetic field.

Figure 6 demonstrates that the outputs of the distributed sensor are in good agreement with that of the MZI measurements for $1200Hz$ sinusoidal magnetic fields for different intensities. A similar experiment at a number of different frequencies verified that the sensor's intensity measurement is independent of the frequency of the applied magnetic field. A resolution of $0.3G$ was determined for the linear region of the plot of figure 6 which corresponds to strain resolution of $0.05\mu\varepsilon$.

The nonlinear response of the sensor to high magnetic fields shown in diagram 6 occurs due to nonlinear response of the Nickel wire. In order to evaluate this nonlinear behavior for magnetic fields with intensity higher than $7G$, it is important to note that the distributed sensor measures the average intensity of the magnetic field along $1m$ of the sensing fibre. Consequently, while a large portion of the sensing fibre is exposed to magnetic field with moderate intensity, the portion of the sensing fibre in the middle of the solenoids experience magnetic field with much higher intensity. Therefore, the nonlinear response to the applied magnetic field starts from those regions of the sensing fibre an it spreads out towards the regions outside the solenoids as the intensity of the magnetic field increases.

The maximum detectable magnetic field of the sensor is a function of the length of the sensing fibre and the frequency of the applied magnetic field. The relationship between the maximum detectable frequency, $f_{B(max)}$, and a fibre sampling rate of S is given by [7]

$$S = 4\pi \times f_{B(max)} \times N_{fringe} \qquad (3)$$

where N_{fringe} is the fringe count at the output of the MZI and represents the amplitude of the magnetic field. The maximum sampling rate of the sensor is limited by the round trip time of the light within the sensing fibre. For a sensor with a $1km$ sensing fibre, maximum fibre sampling rate is $100kHz$. Therefore, the maximum detectable frequency for $8G$ magnetic field is $\sim 7.2kHz$ using equation (3). For a fixed sampling rate, the trade-off between the maximum detectable frequency and the maximum detectable intensity of the applied magnetic field can be obtained from this equation. The sensing range of the sensor can be modified either by using materials with different magnetostrictive constant or by changing the spatial resolution of the sensor. For instance, the sensor can be modified to detect stronger magnetic fields by using a wire with lower magnetostrictive constant or by increasing the spatial resolution of the sensor in order to reducing the strain within the gauge length of the sensor.

Figure 7 demonstrates a good correlation between the sensor and MZI outputs. Since discrete data are used
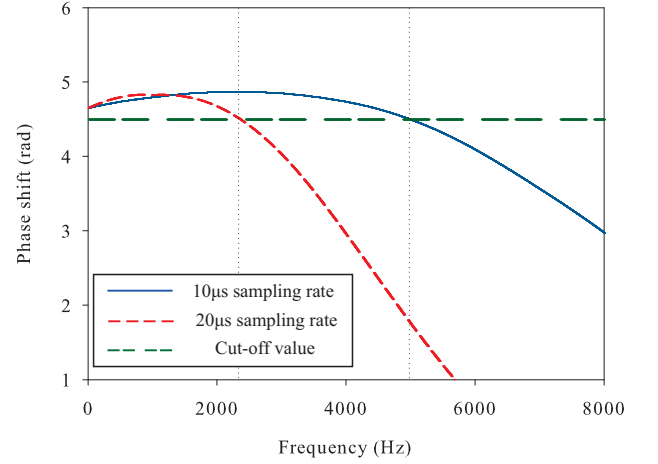

Fig. 8. The differentiate and cross-multiplying demodulator frequency response to an input signal with 1.5π phase-shift at sampling rate of $10\mu s$ (solid blue line) and $20\mu s$ red dashed-line.

for the signal processing procedure, it is the differentiate and cross-multiplying demodulator which imposes limitation on the frequency range of the sensor. This limitation is determined by both the sampling rate and the data acquisition time of each experimental run. The frequency range of $50Hz \sim 5000Hz$ was experimentally determined for the sensor. For frequencies lower than $50Hz$ the output of the demodulator is noisy due to the frequency resolution of the demodulator, $\pm 5Hz$, which is determined by the data acquisition period of $200ms$. For frequencies greater than $5000Hz$, on the other hand, the demodulator attenuates the measured signal and hence the measured intensity of the magnetic field. The frequency response of the differentiate and cross-multiplying demodulator to an input signal with 1.5π phase-shift is shown in figure 8 for two different sampling rates. According to this figure, by allowing a tolerance of $\pm 5\%$, the cut-off frequency of the demodulator for sampling rate of $10\mu s$ and $20\mu s$ are $5000Hz$ and $2500Hz$ respectively.

6. Conclusion

A distributed optical fibre dynamic magnetic field sensor has been demonstrated which is capable of quantifying magnetic fields along $1km$ of the sensing fibre with a spatial resolution of $1m$. It has been shown that in its current form the sensor has a frequency range of $50Hz$ to $5000Hz$ and a frequency resolution of $\pm 5Hz$. The sensor has demonstrated an intensity resolution of $0.3G$ ($\equiv 0.05\mu\varepsilon$) over the magnetic field range of $1G$ to $8G$. The proposed technique has the potential to be used in a wide range of magnetic fields from few tens of mG to hundreds of Gauss by changing the compound of the magnetostrictive element in the sensing fibre. This sensor can be used in a variety of applications ranging from monitoring the state of electrical motors or generators

to detecting distributed magnetic anomalies.

References

[1] A. J. Rogers, "Polarization-optical time domain reflectometry: a technique for the measurement of field distributions," Appl. Optics **20**, 1060-1074 (1981).

[2] L. Palmieri and A. Galtarossa, "Distributed fiber optic sensor for mapping of intense magnetic fields based on polarization sensitive reflectometry," Proc. of SPIE **8351**, 835131 (2012).

[3] S. C. Rashleigh, "Magnetic-field sensing with a single-mode fiber," Opt. Lett. **6**, 19-21 (1981).

[4] A. Yariv and H. V. Winsor, "Proposal for detection of magnetic fields through magnetostrictive perturbation of optical fibers," Opt. Lett. **5**, 87-89 (1980).

[5] P. M. Cavaleiro, F. M. Araujo, and A. B. L. Ribeiro "Metal-coated fibre Bragg grating sensor for electric current metering," Electron. Lett. **34**, 1133 - 1135 (1998).

[6] M. Li, J. Zhou, Z. Xiang, and F. Lv, "Giant magnetostrictive magnetic fields sensor based on dual fiber Bragg gratings," Networking, Sensing and Control IEEE Proc., 490-495 (2005).

[7] A. Masoudi, M. Belal, and T. P. Newson, "A distributed optical fibre dynamic strain sensor based on phase-OTDR," Meas. Sci. Technol. **24**, 085204 (2013).

[8] R. G. Priest, "Analysis of fiber interferometer utilizing 3×3 fiber coupler," IEEE J. Quantum Electron. **18**, 1601-1603 (1982).

[9] C. B. Cameron, R. M. Keolin, and S. L. Garrett, "A symmetrical analog demodulator for optical fiber interferometric sensors," Proc. 34th Midwest symposium on circuits and systems **2**, 666 (1992).